

Heterobimetallic Lantern Complexes That Couple Antiferromagnetically through Noncovalent Pt...Pt Interactions

Frederick G. Baddour,[†] Stephanie R. Fiedler,[‡] Matthew P. Shores,[‡] James A. Golen,[§] Arnold L. Rheingold,[§] and Linda H. Doerrer^{*,†}

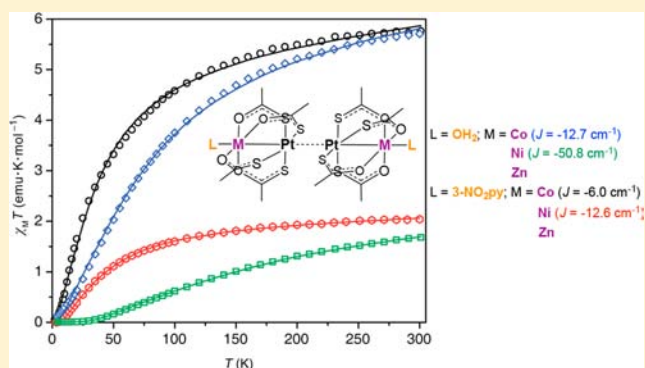
[†]Department of Chemistry, Boston University, Boston, Massachusetts 02215, United States

[‡]Department of Chemistry, Colorado State University, Fort Collins, Colorado 80523, United States

[§]Department of Chemistry and Biochemistry, University of California, San Diego, La Jolla, California 92093, United States

Supporting Information

ABSTRACT: A series of Pt-based heterobimetallic lantern complexes of the form [PtM(SAc)₄(OH₂)] (M = Co, **1**; Ni, **2**; Zn, **3**) were prepared using a facile, single-step procedure. These hydrated species were reacted with 3-nitropyridine (3-NO₂py) to prepare three additional lantern complexes, [PtM(SAc)₄(3-NO₂py)] (M = Co, **4**; Ni, **5**; Zn, **6**), or alternatively dried in vacuo to the dehydrated species [PtM(SAc)₄] (M = Co, **7**; Ni, **8**; Zn, **9**). The Co- and Ni-containing species exhibit Pt—M bonding in solution and the solid state. In the structurally characterized compounds **1–6**, the lantern units form dimers in the solid state via a short Pt...Pt metallophilic interaction. Antiferromagnetic coupling between 3d metal ions in the solid state through noncovalent metallophilic interactions was observed for all the paramagnetic lantern complexes prepared, with *J*-coupling values of -12.7 cm^{-1} (**1**), -50.8 cm^{-1} (**2**), -6.0 cm^{-1} (**4**), and -12.6 cm^{-1} (**5**). The Zn complexes **3** and **6** also form solid-state dimers, indicating that the formation of short Pt...Pt interactions in these complexes is not predicated on the presence of a paramagnetic 3d metal ion. These contacts and the resultant antiferromagnetic coupling are also not unique to heterobimetallic lantern complexes with axially coordinated H₂O or the previously reported thiobenzoate supporting ligand.



INTRODUCTION

It has long been a goal of synthetic chemistry to prepare materials in which rational control can be exerted over the resulting electronic and magnetic properties. The manipulation of magnetic spins has been widely explored in the context of data storage¹ and molecular imaging through MR contrast agents.² A great deal of work has also been conducted in preparing materials that, in addition to useful magnetic and electronic properties, exhibit extended one-dimensional (1D) geometries.³ These pseudo 1D arrays have been used as vapo-chromic sensors,⁴ luminescent materials,^{5,6} and, when partially reduced^{7,8} or oxidized,³ can have anisotropic electrical conductivity.⁹ Recently, multimetal systems have been studied using poly(pyridylamide) ligands to prepare extended metal atom chains (EMACs) with a focus on detailed atomic and electronic structure characterization.¹⁰ The magnetic properties of many EMAC systems have been well studied and strong coupling is often observed between the paramagnetic centers held together by the supporting ligands.^{11,12} Metal–metal interactions can also be formed via the well-studied phenomenon of metallophilicity.^{13–15} These noncovalent M–M interactions can form between closed shell and closed

subshell metal centers affording the widely observed $d^{10}-d^{10}$, $d^{10}-d^8$, and d^8-d^8 combinations.¹⁶

Previously,¹⁷ we reported the synthesis and characterization of a series of heterobimetallic lantern complexes [PtM(tba)₄(OH₂)] (M = Fe, Co, Ni; tba = thiobenzoate) that incorporated high spin 3dⁿ M(II) and low spin 5d⁸ Pt(II) centers. The Co- and Ni-containing compounds exhibited unbridged Pt...Pt interactions in the solid state with antiferromagnetic coupling constants of -10.8 cm^{-1} and -60 cm^{-1} , respectively. These dimers were the first examples of metallophilic interactions facilitating magnetic coupling between unbridged metal atoms. Furthermore, heterobimetallic lantern complexes with metallophilic contacts in the solid state were also a new phenomenon, although metallophilic contacts have been observed with dithiocarboxylate lanterns [Pt₂(S₂CR)₄].^{18–21} Herein we report an extension of our synthetic method to a second thiocarboxylate backbone with different or no axial ligands and demonstrate further examples of close Pt...Pt interactions in the solid state and subsequent

Received: November 19, 2012

Published: April 19, 2013

antiferromagnetic coupling through the established Pt...Pt interactions.

EXPERIMENTAL SECTION

General Considerations. Potassium tetrachloroplatinate (K_2PtCl_4) was prepared from hexachloroplatinic acid (H_2PtCl_6), itself prepared²² from commercially obtained platinum metal and converted to K_2PtCl_4 using a literature procedure.²³ The compound K_2PtCl_4 was then synthesized from K_2PtCl_6 using a literature method.²⁴ All other reagents were obtained commercially and used without further purification. Thermogravimetric analyses (TGA) were conducted with a TA Instruments Q50 thermogravimetric analyzer. Typical data collection parameters include a heating rate of 10 °C/min and a final temperature of 300 °C. UV-vis-NIR spectra were measured between 190 and 1500 nm with a Shimadzu UV-3600 spectrometer. 1H NMR spectra for the Evans method^{25,26} were recorded on a Varian 500 MHz spectrometer. A near saturated solution of the analyte in acetone- d_6 doped with hexamethyldisiloxane was measured with a capillary containing only acetone- d_6 doped with the same concentration of hexamethyldisiloxane. Elemental analyses were performed by Atlantic Microlab Inc. (Norcross, GA 30071)

Magnetic Measurements. Magnetic susceptibility data were collected with a Quantum Design MPMS-XL SQUID magnetometer in the temperature range 2–300 K at an applied field of 1000 Oe. Because of potential compound sensitivity to desolvation, microcrystalline samples were used as-prepared: they were not subjected to further grinding or encasement in a polymer matrix. The as-prepared powder samples were loaded into gelatin capsules, inserted into straws, and tapped to pack the solid in place. The absence of ferromagnetic impurities was confirmed for each sample by observing a linear relationship between magnetization and applied field (0.1–5 T) at 125 K. Data were corrected for the magnetization of the sample holder by subtracting the susceptibility of an empty container and for diamagnetic contributions of the sample by using Pascal's constants.²⁷ Theoretical fits to the susceptibility data for **1**, **2**, **4**, and **5** were obtained using a relative error minimization routine (julX 1.4.1)²⁸ with a Hamiltonian of the form $\hat{H} = -2J\hat{S}_1\cdot\hat{S}_2$. As appropriate, refinements included a correction for temperature independent paramagnetism (TIP) and intermolecular interactions (through a mean field approximation defined by julX as the parameter θ).

Syntheses of [PtCo(SAc) $_4$ (OH $_2$)] (1**), [PtNi(SAc) $_4$ (OH $_2$)] (**2**), [PtZn(SAc) $_4$ (OH $_2$)] (**3**), [PtCo(SAc) $_4$] (**7**), [PtNi(SAc) $_4$] (**8**), and [PtZn(SAc) $_4$] (**9**).** The synthesis of [PtCo(SAc) $_4$ (OH $_2$)] (**1**), was conducted using the procedure developed by our group for the synthesis of platinum-containing heterobimetallic lantern complexes using thioacids.¹⁷ A portion of HSac (68 μ L, 0.964 mmol) was mixed with about 30 mL of water and stirred until a homogeneous mixture was formed and no droplets of HSac were evident. A slight excess of NaHCO $_3$ (85 mg, 1.012 mmol) was then dissolved in about 3 mL of water and added to the reaction mixture. After 5 min a 3 mL aqueous solution of K_2PtCl_4 (100 mg, 0.241 mmol) was added to the reaction mixture. Immediately afterward, a 3 mL aqueous solution of CoCl $_2\cdot 6H_2O$ (57 mg, 0.241 mmol) was added dropwise to the reaction mixture. After about 24 h a gray precipitate was filtered from a colorless solution, washed with water and dried briefly in vacuo. The solid was dissolved in about 30 mL of acetone, filtered over a fine frit, and briefly dried in vacuo to yield a purple solid of [PtCo(SAc) $_4$ (OH $_2$)] $_2\cdot 1/2$ (acetone) composition in 38% recrystallized yield. Pale gray crystals suitable for X-ray crystallography were grown directly from the reaction mixture by employing a W-tube synthesis (illustrated in Scheme S3, Supporting Information). Anal. Calcd. for Pt $_2$ Co $_2$ C $_{17.5}$ H $_{31}$ O $_{10.5}$ S $_8$: C, 17.90; H 2.66; N 0.00%. Found: C, 17.82; H, 2.80; N 0.00%. UV-vis-NIR (acetone) (λ_{max} nm (ϵ_M , cm $^{-1}$ M $^{-1}$)): 492(31), 527(12), 580(8), 1284(3). Evans method (acetone- d_6): 4.93 μ_B . If **1** is extensively dried under high vacuum an insoluble microcrystalline gray solid of composition [PtCo(SAc) $_4$] (**7**), is generated in quantitative yield. Thermogravimetric analysis (TGA) details are provided in the Supporting Information. Anal. Calcd for

PtCoC $_8$ H $_{12}$ O $_4$ S $_4$: C, 17.33; H, 2.18; N, 0.00%. Found: C, 17.52; H, 2.18; N, 0.00%.

To obtain [PtNi(SAc) $_4$ (OH $_2$)] (**2**), CoCl $_2\cdot 6H_2O$ was substituted with NiCl $_2\cdot 6H_2O$ in the above synthesis. A yellow-green solid was obtained in 87% crude yield, and recrystallized from acetone/hexanes to obtain analytically pure material of the composition [PtNi(SAc) $_4$ (OH $_2$)] $_2\cdot 1/3$ acetone. Green crystals large enough for single-crystal X-ray diffraction were grown directly from the reaction mixture by performing the reaction in a modified W-tube. Anal. Calcd for Pt $_2$ Ni $_2$ C $_{17}$ H $_{30}$ O $_{10.3}$ S $_8$: C, 17.54; H 2.60; N 0.00%. Found: C, 17.38; H, 2.78; N, 0.00%. UV-vis-NIR (acetone) (λ_{max} nm (ϵ_M , cm $^{-1}$ M $^{-1}$)): 503(3)(sh), 703(6), 812(3), 1387(8). Evans method (acetone- d_6): 2.84 μ_B . If the recrystallized solid is dried extensively under high vacuum an insoluble yellow solid of composition [PtNi(SAc) $_4$] (**8**), is formed in quantitative yield, as shown by TGA (Supporting Information). Anal. Calcd. PtNiC $_8$ H $_{12}$ O $_4$ S $_4$: C, 17.34; H, 2.18; N, 0.00%. Found: C, 17.57; H, 2.06; N, 0.00%.

To obtain [PtZn(SAc) $_4$ (OH $_2$)] (**3**), ZnCl $_2$ was used in place of CoCl $_2\cdot 6H_2O$ in the synthesis of **1**. Colorless crystals suitable for X-ray analysis were grown directly from the reaction mixture by employing a W-tube synthesis. The material was washed with water and dried briefly to give a white powder of the composition [PtZn(SAc) $_4$ (OH $_2$)] $_2\cdot 4.5H_2O$ in 87% yield. Anal. Calcd. for PtZnC $_8$ H $_{23}$ O $_9.5$ S $_4$: C, 14.56; H, 3.51; N, 0.00%. Found: C, 14.83 H, 3.90, N, 0.00%. UV-vis-NIR (acetone) (λ_{max} nm (ϵ_M , cm $^{-1}$ M $^{-1}$)): No absorption in acetone 330–1500 nm. 1H NMR (δ , ppm, {acetone- d_6 }: 2.26 (s, -CH $_3$). $^{13}C\{^1H\}$ NMR (δ , ppm, {acetone- d_6 }: 214.99 (s, C(CH $_3$)), 32.74 (s, C(CH $_3$)). If **3** is dried extensively under high vacuum an insoluble white solid of composition [PtZn(SAc) $_4$] (**9**), is generated, as shown by TGA (Supporting Information). Anal. Calcd. for PtZnC $_8$ H $_{12}$ O $_4$ S $_4$: C, 17.13; H, 2.16; N, 0.00%. Found: C, 17.21 H, 2.06, N, 0.00%.

Synthesis of [PtCo(SAc) $_4$ (3-NO $_2$ py)] (4**), [PtNi(SAc) $_4$ (3-NO $_2$ py)] (**5**), and [PtZn(SAc) $_4$ (3-NO $_2$ py)] (**6**).** To synthesize **4**, freshly prepared [PtCo(SAc) $_4$ (OH $_2$)] (**1**), (276 mg, 0.482 mmol) was dissolved in about 5 mL of acetone and diluted with approximately 50 mL of CH $_2$ Cl $_2$. An amount of 3-nitropyridine (120 mg, 0.964 mmol) was dissolved in about 2 mL of CH $_2$ Cl $_2$ and added slowly to the above mixture while rapidly stirring. The reaction mixture was stirred for 3 h at room temperature. The solvent was removed with a rotary-evaporator, and the brown solid was transferred to a fine-fritted Hirsch funnel in a slurry of ethanol. The solid was washed with ethanol and dried in vacuo. The solid was then recrystallized from CH $_2$ Cl $_2$ and ethanol affording a brown solid with a 47% recrystallized yield. Large brown crystals suitable for single crystal X-ray analysis were obtained from the slow evaporation of a saturated solution of CH $_2$ Cl $_2$. Anal. Calcd. for PtCoC $_{13}$ H $_{16}$ N $_2$ O $_6$ S $_4$: C, 23.01; H, 2.38; N, 4.13%. Found: C, 22.98; H, 2.47; N, 4.03%. UV-vis-NIR(CH $_2$ Cl $_2$) (λ_{max} nm (ϵ_M , cm $^{-1}$ M $^{-1}$)): 266(37,300), 395(405)(sh), 487(128), 520(39), 573(19), 1233(5). Evans method (CDCl $_3$): 5.06 μ_B .

To prepare [PtNi(SAc) $_4$ (3-NO $_2$ py)] (**5**), freshly prepared [PtNi(SAc) $_4$ (OH $_2$)] (**2**), was used in place of [PtCo(SAc) $_4$ (OH $_2$)] (**1**), and the same method was executed. Large green crystals suitable for single crystal X-ray analysis were obtained from the slow evaporation of a saturated solution in CH $_2$ Cl $_2$. Recrystallized yield: 56%. Anal. calcd. for PtNiC $_{13}$ H $_{16}$ N $_2$ O $_6$ S $_4$: C, 23.02; H, 2.38; N, 4.13%. Found: C, 23.08; H, 2.19; N, 4.12%. UV-vis-NIR(CH $_2$ Cl $_2$) (λ_{max} nm (ϵ_M , cm $^{-1}$ M $^{-1}$)): 255(35,700), 334(2423), 660(10), 828(2), 1178(9). Evans method (CDCl $_3$): 3.05 μ_B .

To obtain [PtZn(SAc) $_4$ (3-NO $_2$ py)] (**6**), freshly prepared [PtZn(SAc) $_4$ (OH $_2$)] (**3**), was used instead of [PtCo(SAc) $_4$ (OH $_2$)] (**1**) while following the same procedure outlined above. Large colorless crystals suitable for single crystal X-ray analysis were grown from ether diffusion into a concentrated solution in CH $_2$ Cl $_2$. Recrystallized yield: 30%. Anal. Calcd. for PtZnC $_{13}$ H $_{16}$ N $_2$ O $_6$ S $_4$: C, 22.79; H, 2.35; N, 4.09%. Found: C, 22.73; H, 2.16; N, 4.08%. UV-vis-NIR (CH $_2$ Cl $_2$) (λ_{max} nm (ϵ_M , cm $^{-1}$ M $^{-1}$)): 262(35,500). 1H NMR (δ , ppm, {CDCl $_3$ }) (See Scheme S1, in the Supporting Information, for labeling scheme): 9.83 (d, $^4J = 2.00$ Hz, 1H, H $_1$), 9.31 (d, $^3J = 5.00$ Hz, 1H, H $_2$), 8.80 (d, $^3J = 8.50$ Hz, 1H, H $_3$), 7.86 (dd, $^3J = 8.50$ Hz, $^2J = 5.00$ Hz, 1H, H $_4$),

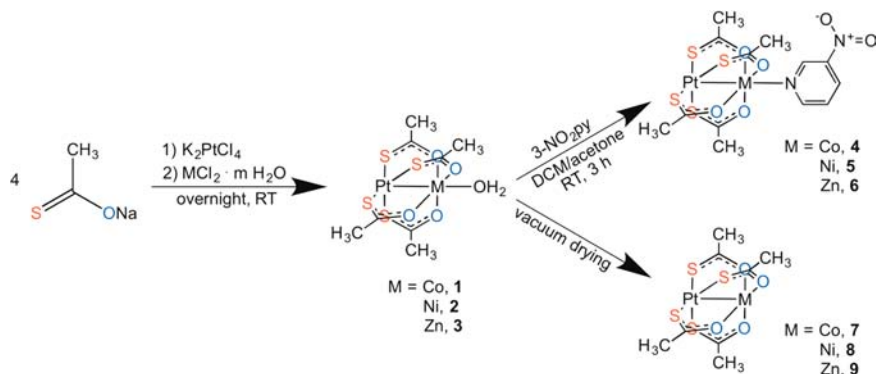
Scheme 1. Synthesis of [PtM(SAc)₄(L)] Compounds

Table 1. Selected Physical Parameters of 1–3 and 4–6

compound	NIR Abs. (nm)	Pt...Pt (Å)	Pt—M (Å)	J coupling (cm ⁻¹)	average SPt...PtS dihedral angle, τ (deg)	average S...S contact (Å)
[PtCo(SAc) ₄ (OH ₂)], 1	1284	3.1261(3)	2.6343(5)	-12.7	45.0(8.2)	3.62(16)
[PtNi(SAc) ₄ (OH ₂)], 2	1387	3.0794(6)	2.585(2)	-50.8	45.0(8.2)	3.58(16)
[PtZn(SAc) ₄ (OH ₂)], 3		3.1246(3)	2.6477(6)		45.0(8.8)	3.62(17)
[PtCo(SAc) ₄ (3-NO ₂ py)], 4	1233	3.489(2)	2.6347(4)	-6.0	0.7(0.1)	3.44(2)
[PtNi(SAc) ₄ (3-NO ₂ py)], 5	1178	3.0583(4)	2.5682(9)	-12.6	45.0(1.7)	3.59(7)
[PtZn(SAc) ₄ (3-NO ₂ py)], 6		3.4453(2)	2.6283(3)		0.5(0.1)	3.44(3)

2.42 (s, 12H, H₃). ¹³C{¹H} NMR (δ , ppm, {CDCl₃}) (See Scheme S2, in the Supporting Information, for labeling scheme): 215.54 (s, C₁), 154.76 (s, C₂), 145.92 (s, C₃), 145.34 (s, C₄), 134.21 (s, C₅), 125.50 (s, C₆), 33.07 (s, C₇).

Single Crystal X-ray Diffraction. All crystals were mounted on a Cryloop with Paratone-N oil and data were collected at 100 K with a Bruker CMOS detector using Mo K α radiation unless otherwise noted. Data were corrected for absorption with SADABS. All non-hydrogen atoms were refined anisotropically by full matrix least-squares on F^2 . All hydrogen atoms, unless specifically addressed, were placed in calculated positions with appropriate riding positions.

Crystals of 1–3 are pale to colorless thin plates, and their structures were solved by direct methods. Hydrogen atoms of water were found from a Fourier difference map, and their distances were fixed at 0.86(2) Å and refined isotropically with 1.20 U_{eq} of parent O atom. The structures of 2 and 3 were solved by direct methods and also by isomorphous replacement using the structural solution of 1. Residual electron density was found near Pt and S of 2 and 3, which has been attributed to lack of analytical absorption correction, quality of crystal, and the nature of the detector. Esd values for the C–C distances of 2 are rather high and indicate that the quality of data is low.

The structures of 4–6 were all solved by direct methods, and the crystal colors are light-brown, green, and colorless, respectively. Data for compound 5 were collected using a Bruker APEX II detector, and the Platon program SQUEEZE²⁹ was employed to resolve unrefined solvent. The program found a void of 971 Å³ and 383 e⁻. This density was associated with eight molecules of dichloromethane (336 e⁻) and 8 C, 16 H, and 16 Cl were added to the unit card to adjust the chemical formula, molecular mass, density, and F000 value.

RESULTS AND DISCUSSION

Synthesis and Structural Characterization. Thioacetate was chosen as a ligand for the preparation of heterobimetallic lantern complexes because, like thiobenzoate,¹⁷ its two different binding moieties allow it to selectively bind Pt and first-row transition metals at different sites and minimize ligand exchange. The change from a phenyl to methyl thioacrylate substituent would test the relative influence of intermolecular van der Waals forces on the formation of metallophilic contacts. It has previously been shown in the family of compounds

[Pt₂(S₂CR)₄] that longer alkane substituents such as R = C₄H₉ give rise to short Pt...Pt contacts (3.12 Å) in the solid state that are not observed when R = CH₃ suggesting that ligand-based vdW interactions can play a role in the formation of Pt...Pt contacts.²⁰ Very few heterobimetallic lantern complexes of the form [PtM(L₄X₄)] with 3d metals have been reported in the literature. Previous examples use 2-mercapto-4-methylpyridine (Me-mpy), [PtM(Me-mpy)₄(NCCH₃)],^{30,31} (M = Co, Ni) and ϵ -thiocaprolactam (tc), [PtCr(tc)₄] and [PtCr(tc)₄Cl].³² There are also few reports of lantern complexes prepared with thioacetate, consisting only of the homobimetallic [Ni₂(SAc)₄(EtOH)],³³ and only one example, [Rh₂(SAc)₄(HSac)₂],³⁴ of a structurally characterized species.

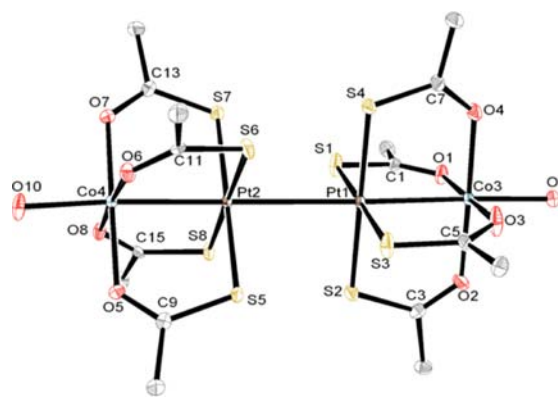
The synthesis of [PtM(SAc)₄(OH₂)] compounds as shown in Scheme 1 is analogous to our previous report on the synthesis of heterobimetallic lantern complexes with thio-benzoate.¹⁷ A solution of sodium thioacetate was prepared in situ and reacted first with an aqueous solution of K₂PtCl₄ with the subsequent addition of a first-row transition metal chloride hydrate to yield [PtM(SAc)₄(OH₂)] (M = Co, 1; Ni, 2; Zn, 3). Compounds 1–3 undergo axial ligand exchange upon reaction with 2 equiv of 3-NO₂py in a mixture of acetone/CH₂Cl₂ to yield [PtM(SAc)₄(3-NO₂py)] (M = Co, 4; Ni, 5; Zn, 6). Alternatively, 1–3 could be converted into the insoluble powders [PtM(SAc)₄] (M = Co, 7; Ni, 8; Zn, 9) if extensively dried under vacuum. Only 2 underwent a color change upon desolvation changing from green to yellow upon vacuum treatment. Crystals suitable for single-crystal X-ray diffraction studies were obtained by conducting the reaction in a W-tube for 1–3 and by recrystallization from CH₂Cl₂ for compounds 4–6.

Compounds 1–6 were crystallographically characterized, and the data collection parameters are summarized in Table 3. Single-crystal X-ray diffraction studies of 1 reveal a dimeric structure, shown in Figure 1, with an average Pt–Co distance of 2.629(7) Å and a short Pt...Pt contact of 3.1261(3) Å. There are no bridging atoms between the two [PtCo(SAc)₄(OH₂)]

Table 2. Pt(II) Compounds That Exhibit Very Short Intermolecular Pt...Pt Distances

compound	intermolecular Pt...Pt dist. (Å)	ref.
[Pt(dmgl) ₂]	3.0391(3)	40
[(en)Pt(SO ₂ O) ₂ Pt(en)]·3H ₂ O	3.0441(7)	39
{[(en)Pt(μ-OH) ₂ Pt(en)]Ag(NO ₃) ₂ NO ₃ }	3.0542(9)	41
[PtNi(SAc) ₄ (3-NO ₂ py)], 5	3.0583(4)	this work

units, and they are rotated by approximately 45° from one another resulting in a staggered conformation. This staggered conformation leads to close S...S contacts between lanterns with an average S–S separation of 3.62(16) Å. One H₂O molecule is bound to each Co center with distinct Co–O distances of 2.082(2) and 2.069(2) Å at the termini of the tetrametallic unit. Selected characterization data of **1–3** and **4–6** are summarized in Table 1. The average dihedral angle (τ) is reported to quantify the relative lantern orientations and was calculated for eight S–Pt...Pt–S dihedral angles in the staggered structures of **1–3**, **5**, and the associated standard deviation is reported. Only four angles are included in the average value for the eclipsed structures of **4** and **6**. Compounds **2** and **3** are isostructural to **1** existing as dimers of lanterns in the solid state. Compound **2** (Figure S1, Supporting Information) exhibits a shorter Pt...Pt contact of 3.0794(6) Å and an average Pt–Ni distance of 2.578(10) Å. The S...S contacts in **2** are slightly shorter with an average separation of 3.58(16) Å. Compound **3** (Figure S2, Supporting Information) displays an intermediate Pt...Pt distance of 3.1246(3) Å, an average Pt–Zn distance of 2.369(12) Å, and with an average S...S distance of 3.62(17) Å. The intramolecular distances (shown in Table 1) are generally unexceptional except that very few intramolecular Pt–M lantern distances are known because of the previous scarcity of such heterobimetallic complexes. These Pt...M distances are comparable to those in the thiobenzoate derivatives,¹⁷ as well as to those observed in the related methyl-cytosine bridged CuPtCu species³⁵ and several heterotrimeric complexes

**Figure 1.** ORTEP of [PtCo(SAc)₄(OH₂)₂·4H₂O, **1**. Ellipsoids are drawn at the 50% level. Waters of crystallization and hydrogen atoms have been removed for clarity.

bridged by amidate ligands.^{36,37} The compounds with O/N donor ligands do not form metallophilic contacts, however, because of the additional substituents on the N donor atoms. All Pt...M distances observed in **1–6** fall well within the range of literature distances as determined by a search of the Cambridge Structural Database³⁸ that included strictly Pt(II)...M(II) intramolecular distances (no μ_2 -X ligands) below 3.0 Å revealing average distances (Å) of 2.60(9) for Pt...Co (11 distances in 9 structures), 2.59(4) for Pt...Ni (12 distances in 7 structures), and 2.74(7) for Pt...Zn (6 distances in 3 structures).

When the axial H₂O molecule is substituted by the 3-NO₂py ligand, as in the cases of **4–6**, the Pt...Pt distance observed in the solid state varies more than in **1–3**. Complex **4** exists as a dimer structure as shown in Figure 2; however, a longer Pt...Pt distance of 3.489(2) Å is observed, and the lantern units are notably offset from one another as indicated by a Pt(1)—Pt(1')—Co(1) angle of 160.76(1)°, in which an angle of 180° would be indicative of a perfectly linear arrangement of lantern units, and **1** has an angle of 179.45(1)°. In addition to this deviation from linearity, the lantern units in **4** have an eclipsed configuration, with two close S...S contacts between S(1)—

Table 3. Summary of X-ray Crystallographic Data Collection Parameters

compound	1	2	3	4	5	6
formula	C ₈ H ₁₈ CoO ₇ PtS ₄	C ₈ H ₁₈ NiO ₇ PtS ₄	C ₈ H ₁₈ O ₇ PtS ₄ Zn	C ₁₃ H ₁₆ CoN ₂ O ₆ PtS ₄	C ₁₃ H ₁₆ N ₂ NiO ₆ PtS ₄ , CH ₂ Cl ₂	C ₁₃ H ₁₆ N ₂ O ₆ PtS ₄ Zn
formula weight	608.48	608.26	614.92	678.54	763.24	684.98
crystal system	triclinic	triclinic	triclinic	monoclinic	monoclinic	monoclinic
space group	<i>P</i> $\bar{1}$	<i>P</i> $\bar{1}$	<i>P</i> $\bar{1}$	<i>P</i> 2(1)/ <i>c</i>	<i>P</i> 2(1)/ <i>n</i>	<i>P</i> 2(1)/ <i>c</i>
<i>a</i> , Å	8.3411(7)	8.2929(6)	8.3518(5)	8.4702(3)	18.6945(7)	8.4935(5)
<i>b</i> , Å	14.1061(12)	14.0255(10)	14.0884(8)	12.2601(4)	8.7141(4)	12.2649(7)
<i>c</i> , Å	16.1443(14)	16.0661(12)	16.105(9)	19.8667(6)	29.5850(13)	19.6930(11)
α , deg	66.951(3)	66.751(2)	66.929(2)	90	90	90
β , deg	88.436(3)	88.460(2)	88.434(2)	94.0470(1)	101.960(2)	93.712(3)
γ , deg	87.007(3)	87.302(2)	86.826(2)	90	90	90
<i>V</i> , Å ³	1745.5(3)	1715.0(2)	1740.71(17)	2057.92(12)	4714.9(3)	2047.2(2)
<i>Z</i>	4	4	4	4	8	4
ρ (calcd), g cm ⁻³	2.316	2.356	2.346	2.190	2.150	2.222
μ (Mo <i>K</i> α), mm ⁻¹	9.457	9.756	9.908	8.034	7.340	8.437
temp, K	100(2)	100(2)	100(2)	100(2)	100(2)	100(2)
<i>R</i> (<i>F</i>), % ^a	2.14	5.81	3.34	2.31	4.23	1.91
<i>R</i> (ωF^2), % ^b	5.19	18.30	7.10	4.89	11.13	3.81

^a $R = \sum |F_o| - |F_c| / \sum |F_o|$. ^b $R(\omega F^2) = \{ \sum [\omega(F_o^2 - F_c^2)^2] / \sum [\omega(F_o^2)^2] \}^{1/2}$; $\omega = 1 / [\sigma^2(F_o^2) + (aP)^2 + bP]$ with *a* and *b* given in CIF, $P = [2F_c^2 + \max(F_o, 0)] / 3$.

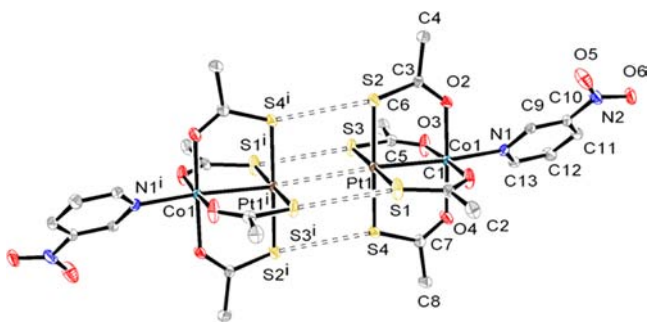


Figure 2. ORTEP of $[\text{PtCo}(\text{SAC})_4(3\text{-NO}_2\text{py})]_2$, **4**. Ellipsoids are drawn at the 50% level. Hydrogen atoms have been removed for clarity.

$\text{S}(3^i)$ of 3.425(1) Å and 3.460(1) Å for $\text{S}(2) \cdots \text{S}(4^i)$, and an average $\text{S} \cdots \text{Pt} \cdots \text{Pt} \cdots \text{S}$ dihedral angle near zero. This structure is contrary to that of **5**, wherein linearity has been restored (Figure S3, Supporting Information) with a $\text{Pt}(1) \cdots \text{Pt}(2) \cdots \text{Ni}(2)$ angle of $178.33(2)^\circ$. The conformation of **5** is staggered, much like what is observed for **1–3**. The $\text{Pt} \cdots \text{Pt}$ distance of 3.0583(4) Å is exceptionally short, with only three examples reported that exhibit shorter^{39–41} contacts between strictly Pt(II) centers as shown in Table 2. Despite having an exceptionally short $\text{Pt} \cdots \text{Pt}$ distance, **5** exhibits the longest $\text{S} \cdots \text{S}$ contacts between lanterns, with an average separation of 3.59(7) Å. Complex **6** (Figure S4, Supporting Information) is isostructural to **4**, with a $\text{Pt}(1) \cdots \text{Pt}(1^i) \cdots \text{Zn}(1)$ angle of 159.36° and a $\text{Pt} \cdots \text{Pt}$ and an average $\text{S} \cdots \text{S}$ distance of 3.4453(2) and 3.44(2), respectively Å.

Other two-electron Lewis base donors, L, can be prepared in these $[\text{PtM}(\text{SAC})_4\text{L}]$ systems, but these do not result in dimerization via the $\text{Pt} \cdots \text{Pt}$ interactions, as will be discussed in detail in a future report.

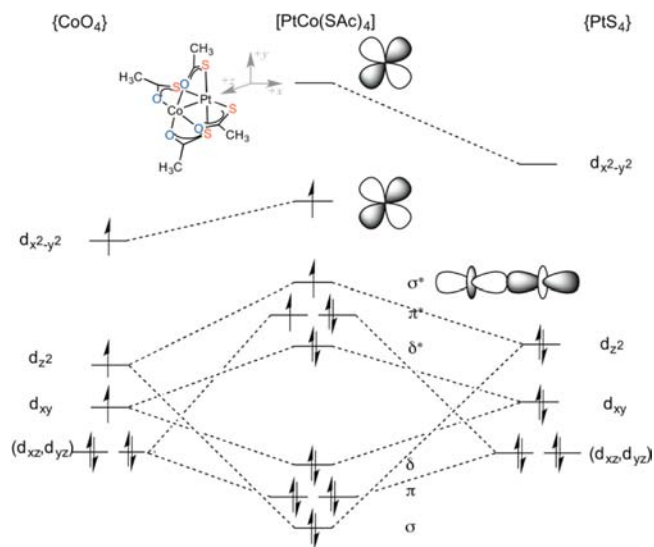
Electronic Structure. Of the previously reported thioacetate lantern compounds, only the homometallic nickel species exhibit homoleptic coordination as observed in **1–6**. In the case of $[\text{Rh}_2(\text{SAC})_4(\text{HSAC})_2]$ each rhodium center has $\{\text{RhO}_2\text{S}_3\}$ coordination from thioacetate and thioacetic acid ligands.³⁴ Notably, the solid-state diffuse reflectance spectrum³³ of $[\text{Ni}_2(\text{SAC})_4(\text{EtOH})]$ has a low-energy absorption feature at 1299 nm, which is consistent with a weak intermetallic d–d transition. A weak ($3\text{--}10 \text{ cm}^{-1} \text{ mol}^{-1}$) intermetallic d–d transition was also observed¹⁷ in $[\text{PtM}(\text{tba})(\text{OH}_2)]$ complexes appearing at 1275 and 1337 nm for Co and Ni respectively.

Spectroscopic and magnetic susceptibility data for **1–6** are consistent with monomeric complexes in solution analogous to the previously reported thioacetate derivatives.¹⁷ Ligand-to-metal charge transfer bands in the UV region of 266, 255, and 262 nm are observed for **4–6** respectively. These UV transitions could not be recorded for compounds **1–3** because of decomposition in solvents with an appropriate energy window to collect this region of the UV spectrum. Because this feature is observed for the three different metal compounds, a $\sigma(\text{PtM})$ to $\sigma^*(\text{PtM})$ transition, of the type characterized in $\text{Pt}(\text{III})_2$ and $\text{Rh}(\text{II})_2$ dimers, was ruled out.⁴² Ligand-to-metal charge transfer (LMCT) features of water and acetate to Pt in lantern structures have been observed (and assigned by calculation) at 317 and 363 nm,⁴² and higher energy LMCT absorptions for O–M(3d) species are reasonable. The related dithiocarboxylate compound, $[\text{Pt}_2(\text{S}_2\text{CCH}_3)_4]$ exhibits two absorption features near 260 nm, one at 263 nm and another at 265 nm with ϵ values of approximately 10^4 .⁴³ Therefore a S–

Pt LMCT could also be contributing to the absorptions observed near 260 nm. Cobalt-containing complexes **1** and **4** each exhibit three characteristic absorbances in the visible region with those of **1** observed at 492, 527, and 580 nm. These metal-to-ligand charge-transfer (MLCT) bands are blue-shifted by approximately 6 nm when the axial ligand is changed from water in **1** to 3- NO_2py in **4**. Two major MLCT bands are present in the electronic spectra of the Ni-derivatives, appearing at 703 and 812 nm for **1** and 660 and 828 nm for **5**. Compounds **1** and **2** and their 3- NO_2py derivatives **4** and **5** all exhibit weak NIR absorptions in solution that can be assigned to a weak intermetallic d–d transition shown in Table 1. This assignment is further supported by the absence of a NIR transition in the prepared Zn-derivatives, **3** and **6**, in which the d^{10} character of Zn eliminates the possibility for this transition to occur. Similar to N-donors in $[\text{Ni}_2(\text{SAC})_4(\text{L})]$, substitution of 3- NO_2py for H_2O results in a blue shift of the NIR d–d absorption band.

The qualitative molecular orbital (MO) picture shown in Scheme 2 of Pt–Co in the heterobimetallic lantern subunits is

Scheme 2. MO Diagram for Pt–Co Interaction in $[\text{PtCo}(\text{SAC})_4\text{L}]$



analogous to what was found in the $[\text{PtM}(\text{tba})_4]$ series in geometry-optimized spin-unrestricted density functional theory (DFT) calculations.¹⁷ The sides of Scheme 2 illustrate the qualitative ligand-field splitting of the $\{\text{CoO}_4\}$ unit with a high-spin configuration and the low-spin environment of the $\{\text{PtS}_4\}$ fragment. The center of Scheme 2 shows how the overlap of the two square planar $\{\text{CoO}_4\}$ and $\{\text{PtS}_4\}$ fragments results in a new high-spin lantern system. This qualitative MO description is used to attribute tentatively the observed weak NIR absorptions to a M-to-Pt charge transfer into the hypothesized Pt-based $d_{x^2-y^2}$ lowest unoccupied MO (LUMO) as shown in Scheme 2. Because the NIR absorbances have small extinction coefficients, they have not been assigned to any spin and parity allowed transitions, such as a π^* to σ^* . The diagram also provides an illustrative example of the antibonding M–Pt MOs, for example, the σ^* MO, whose intermolecular overlap enable Pt–Pt electronic communication. Stronger intramolecular interaction between the M- and Pt-orbitals results in greater electron density in the Pt-based antibonding orbitals and therefore stronger intermolecular Pt–Pt coupling.

Magnetic Properties. The Evans method solution phase susceptibility values of 4.93 (1), 2.84 (2), 5.06 (4), and 3.05 μ_B (5) are consistent with monomeric {MPT} species in solution in which high spin first-row transition metal centers are bound to the oxygen donor atoms of the thiocarboxylate moieties in pseudo-octahedral coordination geometries.

The solid-state magnetic susceptibility data for the species containing crystallographically characterized apical ligands are shown in Figure 3, along with best fits obtained from julX.²⁸

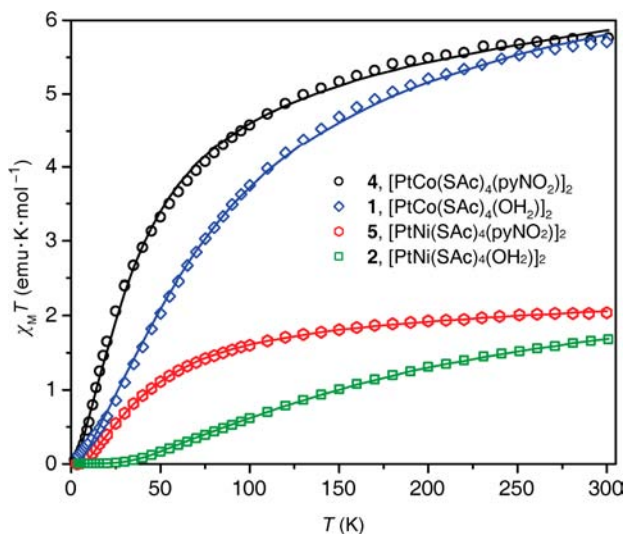


Figure 3. Temperature dependence of magnetic susceptibility for 1–2 and 4–5 measured at 1000 G. In each case, data are treated as M–Pt⋯Pt–M dimer units. The best fits obtained from julX are presented as solid lines. See the text and Supporting Information for a description of the fitting methods and parameters.

The $\chi_M T$ products are presented as {MPT}₂ dimeric units, as observed in our previous report;¹⁷ to interpret these data as {MPT} gives nonsensical results. At 300 K the $\chi_M T$ products for 1 and 4 are 5.71 and 5.74 emu K mol⁻¹, respectively ($\mu_{\text{eff}} = 6.76$ and 6.78 μ_B), higher than expected for two magnetically uncoupled $S = 3/2$ Co(II) centers with $g = 2$ (3.75 emu K mol⁻¹), but consistent with spin–orbit coupling and unquenched orbital contributions to the magnetic susceptibilities.

At 300 K the $\chi_M T$ products for 2 and 5 are 1.68 and 2.04 emu K mol⁻¹ ($\mu_{\text{eff}} = 3.66$ and 4.04 μ_B), respectively. These values are very similar to what would be expected for two uncoupled Ni(II) centers with $g = 2$ (2.00 emu K mol⁻¹). The ambient temperature susceptibilities reflect the first row transition metal ion employed and are not perturbed significantly by the apical ligand.

All four complexes show significant drops in $\chi_M T$ values as the temperature is decreased, consistent with antiferromagnetic coupling of paramagnetic centers to afford singlet ground states. Fitting the susceptibility centers data to an isotropic exchange coupling model (Table 4; details of the fitting procedures are provided in the Supporting Information) allows comparisons of the new complexes with the [PtM(tba)₄(OH₂)₂]₂ species reported previously.¹⁷ Note that an alternate fit of 2 was considered, which included a zero-field splitting term, D , instead of a mean field approximation, θ , but the fit quality did not improve and the coupling, J , remained similar (details are provided in the Supporting Information).

Several trends emerge from a study of the susceptibility data in Table 4. First, the Ni-containing complexes consistently show significantly stronger intramolecular exchange interactions (larger $|J|$) and more isolated behavior (larger $J/|\theta|$) than the Co analogues. This pattern does not seem to be correlated to Pt⋯Pt distances or the S–Pt⋯Pt–S dihedral angle τ , but instead likely reflects differences in M–Pt orbital overlap. Specifically, stronger coupling observed for the Ni-containing complexes suggests better intramolecular M–Pt orbital overlap and more facile intermolecular Pt–Pt coupling. Second, the substitution of thiobenzoate (tba) with thioacetate (SAC) has a moderate but inconsistent effect on the strength of magnetic exchange, as $|J|$ changes by $\sim 17\%$ upon adoption of SAC, but is increased for the Co complex 1 and decreased for the Ni analogue 2. Local structural parameters (Pt⋯Pt distance, {MPT}₂ dihedral angles) are similar for the Ni complexes, and the Pt⋯Pt distance actually increases for the Co complex (tba vs 1), suggesting that the structural changes are not directly responsible for the changes in coupling. Combining both the intra- and the intermolecular exchange terms, one can argue that the SAC ligand decreases coupling overall for both 1 and 2, but packing effects or intermolecular interactions appear to isolate the {CoPt}₂ species better for SAC than tba, resulting in a somewhat larger relative coupling constant (i.e., larger J/θ). Third, the substitution of apical aquo with 3-NO₂py ligands in 4 and 5 significantly reduces the coupling between {MPT} units. It is tempting to add that the 3-NO₂py ligands also increase separation of {MPT}₂ dimers, but that distinction is complicated somewhat by the slightly different structure of 4 compared to the other species.

Given that substitution of aquo for 3-NO₂py reduces coupling, it is interesting to note that complete removal of the aquo ligand does not appear to have the same effect. Variable-temperature susceptibility measurements carried out on the dehydrated 7 (Figure S6, Supporting Information) are virtually identical to those observed for 1. In addition, whereas 8 (lemon yellow) and 2 (yellow-green) have different colors, the susceptibility data (Figure S8, Supporting Information) are very similar. The similarities of the dehydrated and solvated

Table 4. Comparison of Fitted Magnetic Parameters for {MPT}₂ Complexes

compound	J (cm ⁻¹)	g	TIP ($\times 10^{-6}$ emu K mol ⁻¹)	θ (cm ⁻¹)	J/θ	f^a	Pt⋯Pt (Å)	dihedral angle, τ (deg)
1	-12.7	2.6 ^b	1657	-2.5	5.08	0.05719	3.1261(3)	45.0(8.2)
2	-50.8	2.14	500 ^b	-2.3	22.08	0.005845	3.0794(6)	45.0(8.2)
4	-6.0 ^b	2.45 ^b	2181	-0.6	10	0.06782	3.489(2)	0.7(0.1) ^d
5	-12.6	2.04	491	0 ^c	undef	0.00590	3.0583(4)	45.0(1.7)
Co(tba) ^e	-10.8	2.15	3470	-6.4	1.69	0.0335	3.0650(3)	45.0(17.6)
Ni(tba) ^e	-60	2.187	1220	0 ^c	undef	0.00389	3.0823(4)	45.0(5.6)

^aSum of the deviation squared. ^bFixed parameter. ^cParameter refined to ~ 0 , so it was fixed at 0. ^dNote PtS₄ faces are slipped. ^eFrom ref 17.

compounds' behavior could suggest a minimal role for the axially coordinated aquo ligands and waters of crystallization; however, the data could also indicate that the M centers find thiocarboxylate S or O donor atoms to complete their coordination sphere, and the effects of those ligands are similar to water. Efforts to structurally characterize **7**, **8**, and **9** are ongoing.

Apart from the short Pt...Pt interactions in **1**, **2**, **4**, and **5**, alternative pathways for the observed antiferromagnetic coupling could result from other contacts between [PtM(SAc)₄L] lantern units. Hydrogen bonding contacts for **1** and **2** and associated distances are shown in Supporting Information, Figures S11 and S12, respectively. One axial water molecule of **1** forms a hydrogen-bonding interaction with a molecule of lattice water (2.778(4) Å) and to an oxygen from a thiocarboxylate moiety of a neighboring lantern unit (2.744(3) Å), while the other terminal aquo ligand forms H-bonding contacts with two molecules of lattice water (2.839(5), 2.743(4) Å). Compound **2** forms the same hydrogen-bonding contacts as **1**, with the closest lantern-to-lantern hydrogen-bonding interaction being between a terminal water molecule and an oxygen of an adjacent thiocarboxylate moiety (2.76(1) Å). We have previously shown that the presence of hydrogen bonding in [PtM(tba)₄(OH₂)] species cannot be correlated with the degree of antiferromagnetic coupling.¹⁷ This relationship also holds true here as there is a greater degree of antiferromagnetic coupling in **2**, despite longer hydrogen-bonding interactions than are observed in **1**. Furthermore, a hydrogen-bonding pathway for magnetic coupling cannot be operative in **4** and **5** as no hydrogen bonding interactions are present in the lattice.

CONCLUSIONS

In summary, six heterobimetallic lantern compounds, [PtM(SAc)₄(L)] (M = Co, Ni, Zn) have been synthesized and thoroughly characterized. All of the prepared lantern complexes exist as dimers in the solid state linked via close Pt...Pt interactions, through which antiferromagnetic coupling of paramagnetic 3d metal ions occurs. It has been determined that neither the Pt...Pt interaction between lantern complexes nor the resulting antiferromagnetic coupling is an isolated phenomenon of the thiobenzoate supporting ligand,¹⁷ nor is an axially coordinated H₂O required for the formation of the observed tetrametallic units. Additionally, it is clear that the formation of close Pt...Pt contacts between lantern complexes does not require a paramagnetic 3d metal ion as exemplified by the Zn-containing lanterns **3** and **6**. Further studies are underway to delineate the electronic role of the apical and supporting ligands in the engendering of close Pt...Pt contacts in heterobimetallic lantern complexes, and the antiferromagnetic coupling within, to garner synthetic control over these metallic contacts.

ASSOCIATED CONTENT

Supporting Information

Selected interatomic distances and angles for **1**–**6**; NMR labeling schemes; ORTEPs of **2**, **3**, **5**, and **6**; hydrogen bonding interactions of **1**–**3**; variable temperature susceptibility plots. This material is available free of charge via the Internet at <http://pubs.acs.org>.

AUTHOR INFORMATION

Corresponding Author

*E-mail: doerrerr@bu.edu.

Notes

The authors declare no competing financial interest.

ACKNOWLEDGMENTS

We thank NSF-CCF 0829890 (L.H.D.), NSF-CHE 0619339 (NMR spectrometer at Boston University), and NSF-CHE-1058889 (M.P.S.) for funding.

REFERENCES

- (1) *Magnetic Properties of Organic Materials*; Lahti, P. M., Ed.; Marcel Dekker: New York, 1999.
- (2) *Contrast Agents I: Magnetic Resonance Imaging*; Krause, W., Ed.; Springer: New York, 2002.
- (3) *Extended Linear Chain Compounds*; Miller, J. S., Ed.; Plenum Press: New York, 1982; Vol. 1–3.
- (4) Drew, S. M.; Janzen, D. E.; Buss, C. E.; MacEwan, D. I.; Dublin, K. M.; Mann, K. R. *J. Am. Chem. Soc.* **2001**, *123*, 8414–8415.
- (5) White-Morris, R. L.; Olmstead, M. M.; Balch, A. L. *J. Am. Chem. Soc.* **2003**, *125*, 1033–1040.
- (6) Balch, A. *Gold Bull.* **2004**, *37*, 45–50.
- (7) Prater, M. E.; Pence, L. E.; Clérac, R.; Finnis, G. M.; Campana, C.; Auban-Senzier, P.; Jérôme, D.; Canadell, E.; Dunbar, K. R. *J. Am. Chem. Soc.* **1999**, *121*, 8005–8016.
- (8) Finnis, G. M.; Canadell, E.; Campana, C.; Dunbar, K. R. *Angew. Chem., Int. Ed. Engl.* **1996**, *35*, 2772–2774.
- (9) Bera, J. K.; Dunbar, K. R. *Angew. Chem., Int. Ed.* **2002**, *41*, 4453–4457.
- (10) Berry, J. F. In *Multiple Bonds Between Metal Atoms*, 3rd ed.; Cotton, F. A., Murillo, C. A., Walton, R. A., Eds.; Springer: New York, 2005; pp 669–706.
- (11) Rohmer, M.-M.; Liu, I. P.-C.; Lin, J.-C.; Chiu, M.-J.; Lee, C.-H.; Lee, G.-H.; Bénard, M.; López, X.; Peng, S.-M. *Angew. Chem., Int. Ed.* **2007**, *46*, 3533–3536.
- (12) Liu, I. P.-C.; Chen, C.-H.; Chen, C.-F.; Lee, G.-H.; Peng, S.-M. *Chem. Commun.* **2009**, 577–579.
- (13) Jansen, M. *Angew. Chem., Int. Ed. Engl.* **1987**, *26*, 1098–1110.
- (14) Pyykkö, P. *Chem. Rev.* **1997**, *97*, 597–636.
- (15) Schmidbaur, H.; Schier, A. *Chem. Soc. Rev.* **2008**, *37*, 1931–1951.
- (16) Doerrerr, L. H. *Dalton Trans.* **2010**, *39*, 3543–3553.
- (17) Dahl, E. W.; Baddour, F. G.; Fiedler, S. R.; Hoffert, W. A.; Shores, M. P.; Yee, G. T.; Djukic, J.-P.; Bacon, J. W.; Rheingold, A. L.; Doerrerr, L. H. *Chem. Sci.* **2012**, *3*, 602–609.
- (18) Bellitto, C.; Bonamico, M.; Dessy, G.; Fares, V.; Flamini, A. *J. Chem. Soc., Dalton Trans.* **1987**, 35–40.
- (19) Kawamura, T.; Ogawa, T.; Yamabe, T.; Masuda, H.; Taga, T. *Inorg. Chem.* **1987**, *26*, 3547–3550.
- (20) Pérez Paz, A.; Espinosa Leal, L. A.; Azani, M.-R.; Guijarro, A.; Sanz Miguel, P. J.; Givaja, G.; Castillo, O.; Mas-Ballesté, R.; Zamora, F. I.; Rubio, A. *Chem.—Eur. J.* **2012**, *18*, 13787–13799.
- (21) Guijarro, A.; Castillo, O.; Calzolari, A.; Miguel, P. J. S.; Gómez-García, C. J.; di Felice, R.; Zamora, F. I. *Inorg. Chem.* **2008**, *47*, 9736–9738.
- (22) Kauffman, G. B. *Inorg. Synth.* **1967**, *9*, 182–185.
- (23) Keller, R. N. *Inorg. Synth.* **1946**, *2*, 247–250.
- (24) Kauffman, G. B. *Inorg. Synth.* **1963**, *7*, 239–244.
- (25) Evans, D. F. *J. Chem. Soc.* **1959**, 2003–2005.
- (26) Sur, S. K. *J. Magn. Reson.* **1989**, *82*, 169–173.
- (27) Bain, G. A.; Berry, J. F. *J. Chem. Educ.* **2008**, *85*, 532–536.
- (28) Bill, E. *JulX*; Max Planck Institute for Bioinorganic Chemistry: Mülheim an der Ruhr, Germany, 2008; http://www.mpi-muelheim.mpg.de/bac/logins/bill/julX_en.php.
- (29) PLATON, *A Multipurpose Crystallographic Tool*; Utrecht University: Utrecht, The Netherlands, 2005.

- (30) Nishioka, T.; Kinoshita, I.; Ooi, S. i. *Chem. Lett.* **1992**, 883–886.
- (31) Kitano, K. i.; Tanaka, K.; Nishioka, T.; Ichimura, A.; Kinoshita, I.; Isobe, K.; Ooi, S. i. *Dalton Trans.* **1998**, 3177–3182.
- (32) Scott, T. A.; Abbaoui, B.; Zhou, H.-C. *Inorg. Chem.* **2004**, *43*, 2459–2461.
- (33) Melson, G. A.; Crawford, N. P.; Geddes, B. J. *Inorg. Chem.* **1970**, *9*, 1123–1126.
- (34) Dikareva, L. M.; Sadikov, G. G.; Porai-Koshits, M. A.; Golubnichaya, M. A.; Baranovskii, I. B.; Shchelokov, R. N. *Russ. J. Inorg. Chem.* **1977**, *22*, 1093–1094.
- (35) Hegmans, A.; Zangrando, E.; Freisinger, E.; Pichierri, F.; Randaccio, L.; Mealli, C.; Gerdan, M.; Trautwein, A. X.; Lippert, B. *Chem.—Eur. J.* **1999**, *5*, 3010–3018.
- (36) Chen, W.; Liu, F.; Nishioka, T.; Matsumoto, K. *Eur. J. Inorg. Chem.* **2003**, 4234–4243.
- (37) Chen, W.; Matsumoto, K. *Eur. J. Inorg. Chem.* **2002**, 2664–2670.
- (38) Allen, F. H. *Acta Crystallogr., Sect. B: Struct. Sci.* **2002**, *58*, 380–388.
- (39) Krieglstein, R.; Breitingner, D. K.; Liehr, G. *Eur. J. Inorg. Chem.* **2001**, 3067–3072.
- (40) Konno, M.; Okamoto, T.; Shirotani, I. *Acta Crystallogr., Sect. B: Struct. Sci.* **1989**, *45*, 142–147.
- (41) Shen, W.-Z.; Schnebeck, R.-D.; Freisinger, E.; Lippert, B. *Dalton Trans.* **2008**, 4044–4049.
- (42) Stranger, R.; Medley, G. A.; McGrady, J. E.; Garrett, J. M.; Appleton, T. G. *Inorg. Chem.* **1996**, *35*, 2268–2275.
- (43) Bellitto, C.; Flamini, A.; Piovesana, O.; Zanazzi, P. F. *Inorg. Chem.* **1980**, *19*, 3632–3636.